Progress In Electromagnetics Research, PIER 37, 251–287, 2002

SMALL-SLOPE APPROXIMATION METHOD: A FURTHER STUDY OF VECTOR WAVE SCATTERING FROM TWO-DIMENSIONAL SURFACES AND COMPARISON WITH EXPERIMENTAL DATA

G. Berginc

Thalès Optronique
rue Guynemer, BP 55, 78283 Guyancourt Cedex, France

Abstract—This paper deals with the calculation of the scattering cross-section of polarized electromagnetic plane waves from 2-D metallic and dielectric randomly rough surfaces. The scattering cross-section of object is calculated by the Local Small Slope Approximation (SSA), the scattering cross-section is then compared with experimental data. In this paper, second order terms of the SSA method have been numerically implemented in order to obtain accurate results for a large range of slope. In this paper, we consider scattered and incident wave vectors in arbitrary directions, metallic and dielectric materials with complex permittivity. Surfaces are considered with Gaussian probability density functions for surface heights and Gaussian or non-Gaussian correlation functions. The coherent and incoherent components of the electromagnetic intensity for cross- and co-polarization are calculated in the bistatic case and we give several comparisons of the theory with measured data.

1. INTRODUCTION

Much research has been done on the problem of electromagnetic wave scattering from randomly rough surfaces because of many applications in optics, radiophysics, radioastronomy and solid state physics. The problem is divided into three approaches. First, the theoretical works deal with numerical methods of calculating the wave fields scattered from randomly rough surface [1]. These methods consider different approaches of constructing a set of linear equations and solving them numerically. Using supercomputer allows numerical calculations for statistical ensembles of one-dimensional rough surfaces. But dimensions of sets of linear equations can be too large, when we consider three-dimensional scattering problems. It is then interesting to develop analytical models to compute the scattering coefficients of randomly rough surfaces. Analytical models correspond to the second approach. But the scattering problem for randomly rough surfaces has no exact analytic solution. Two basic methods were used before: the perturbation method, which is valid for small values of the Rayleigh parameter, the ratio of roughness height to the incident wavelength, and the Kirchhoff-tangent plane approximation [2, 3] which is valid for small values of the ratio of wavelength to curvature radius of the surface. In the Kirchhoff-tangent plane approximation (KA), the boundary is approximated at each point by a tangent plane. The value of the field and its normal derivative at the boundary are expressed through the incident field and the scattered field is determined using the Helmholtz expression. Another approach can be obtained proceeding from the integral equations. This theory assumes that the interaction of the electromagnetic wave with the roughness is local. The KA has been systematically tested in the 2-D case in [2, 3]. The perturbation method is only applicable to surfaces with small roughness and the Kirchhoff approximation is applicable to surfaces with long correlation length. A combination

of these two methods gives the two-scale approach, which is inaccurate for grazing angles. In this method, we define a large-scale surface where the scattering processes are described in the Kirchhoff-tangent plane approximation and a small-scale surface on which the small-perturbation method is applied. The predictions of this method are dependent on how the surface is defined and partitioned. Some new approaches were suggested, the phase perturbation theory [4], the Full Wave Method proposed by Bahar [5], the second-order Kirchhoff approximation and the Integral Equation Model (IEM) [6–14], the operator expansions [15] and the local and non-local small-slope approximation [16–23]. The small-slope approximation is more computationally tractable than the operator expansions, which requires Monte Carlo simulation. The small-slope approximation (SSA) is an appropriate candidate to bridge the gap between the Kirchhoff approximation and the small-perturbation method. The small-slope approximation is restricted to single-scattering phenomena. The SSA (first and second order) has been systematically tested and compared to the Kirchhoff approximation in [21, 22]. The non-local small-slope approximation is a modification of the small-slope approximation for situations in which multiple scattering from points situated each other at significant distance becomes important.

In this paper, we have implemented numerically the vector case of the small-slope approximation (first and second order) for Gaussian and non-Gaussian randomly rough surfaces. We have chosen to treat metallic and dielectric random rough surfaces with the small-slope approximation method. Calculations are compared with experimental data for metallic and dielectric randomly rough surface. We investigate non-Gaussian correlation functions for 3D-case scattering, which is an important step, when we study electromagnetic scattering from natural surfaces. The paper is organized as follows.

In Section 2, we give an overview and some explanations about the second-order small-slope approximation in the vector case for a two-dimensional dielectric or metallic randomly rough surfaces with Gaussian or non-Gaussian correlation functions. We consider the expression of the incoherent and coherent scattering cross-sections. When comparing experimental measurements of light scattering with numerical computations, it is helpful if the numerical results provide physical insight to the scattering process. For this reason, we have written a numerical code based on the second-order small-slope approximation. Numerical results are presented in section 3 for Gaussian statistics and for non-Gaussian correlation functions. For bistatic cases, we compare numerical results with measures of dielectric and metallic Gaussian samples. Section 4 contains our concluding

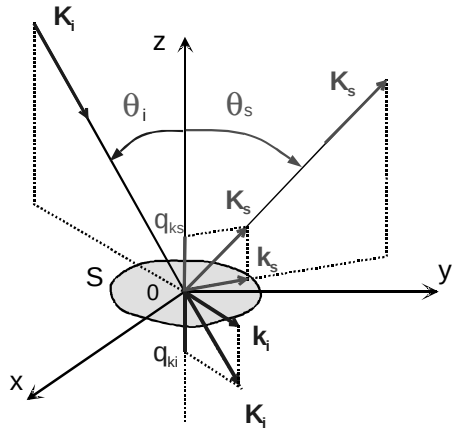

Figure 1. Geometrical configuration for the wave-scattering problem.

remarks.

2. SMALL-SLOPE APPROXIMATION: VECTOR CASE FOR LOCAL INTERACTIONS

The Small-Slope Approximation (SSA) [17, 18] is an analytical approach; its validity is independent of the wavelength of radiation. The slope of surface undulation is smaller than the angles of incidence and scattering. The SSA method gives a solution for wave-scattering problems both at small and large scales within the single theoretical scheme provided that surface roughness has small slope. In this paper, the SSA is formulated in the general form for vector waves. The formulation is given in some detail to emphasize the more complicated nature of vector theory. The three-dimensional scattering problem is treated.

2.1. Expression of the Small-Slope Approximation

The geometrical configuration we adopt to resolve the wave-scattering problem is given in Figure 1. We consider a rough interface $z = h(\mathbf{r})$, with $\mathbf{r} = x\mathbf{u}_x + y\mathbf{u}_y$, between two homogeneous half-spaces which are defined by their permittivity and permeability. The time dependence is assumed to be $\exp(-i\omega t)$.

The rough surface is illuminated by a monochromatic plane-wave coming from the upper half-space defined by $z > 0$. The incident direction is defined by the wave vector $\mathbf{K}_i = \mathbf{k}_i - q_{ki}\mathbf{u}_z$, with

$\mathbf{k}_i = k_{ix}\mathbf{u}_x + k_{iy}\mathbf{u}_y$ and $q_{ki} = \sqrt{K_1^2 - k_i^2}$ where the wave number K_1 in the upper half-space is given by $K_1 = N_1 2\pi/\lambda$ with $N_1 = \sqrt{\mu_1\varepsilon_1}$. λ is the wavelength in the vacuum.

The incident plane-wave is given by:

$$\mathbf{E}^i = \mathbf{e}^i_{\alpha_i}(\mathbf{k}_i)\exp(i\mathbf{k}_i.\mathbf{r} - iq_{ki}z) \tag{1}$$

Where $\mathbf{e}^i_{\alpha_i}(\mathbf{k}_i)$ is the unit vector defining the polarization of the incident wave. It is given for $\alpha_i = 1, 2$, by the following expressions:

$$\mathbf{e}^i_1(\mathbf{k}_i) = -\left(k_i^2\mathbf{u}_z + q_{ki}\mathbf{k}_i\right)\Big/(K_1 k_i) \quad \text{And} \quad \mathbf{e}^i_2(\mathbf{k}_i) = (\mathbf{u}_z \wedge \mathbf{k}_i)\Big/k_i \tag{2}$$

We consider the scattered field in the upper half-space for directions given by the wave vector $\mathbf{K}_s = \mathbf{k}_s + q_{ks}\mathbf{u}_z$, with $\mathbf{k}_s = k_{sx}\mathbf{u}_x + k_{sy}\mathbf{u}_y$ and $q_{ks} = \sqrt{K_1^2 - k_s^2}$. The scattered field is defined as the following plane wave spectrum:

$$\mathbf{E^s} = \int \sum_{\alpha_s=1,2} A_{\alpha_s\alpha_i}(\mathbf{k}_s, \mathbf{k}_i)\mathbf{e}^s_{\alpha_s}(\mathbf{k}_s)\exp(i\mathbf{k}_s{\cdot}\mathbf{r} + iq_{ks}z)d\mathbf{k}_s\Big/(2\pi)^2 \tag{3}$$

Where $A_{\alpha_s\alpha_i}(\mathbf{k}_s, \mathbf{k}_i)$, the scattering amplitude (SA), is the coefficient of the plane wave expansion defined for an incident polarization $\mathbf{e}^i_{\alpha_i}(\mathbf{k}_i)$ and a scattered polarization $\mathbf{e}^i_{\alpha_s}(\mathbf{k}_s)$ given, for $\alpha_s = 1, 2$, by:

$$\mathbf{e}^s_1(\mathbf{k}_s) = -\left(k_s^2\mathbf{u}_z + q_{ks}\mathbf{k}_s\right)\Big/(K_1 k_s) \quad \text{and} \quad \mathbf{e}^s_2(\mathbf{k}_s) = (\mathbf{u}_z \wedge \mathbf{k}_s)\Big/k_s \tag{4}$$

With the four coefficients given for $\alpha_i = 1, 2$ and $\alpha_s = 1, 2$, the scattering process is described by the 2×2 matrix $A_{\alpha_s\alpha_i}(\mathbf{k}_s, \mathbf{k}_i)$:

$$\mathbf{A}(\mathbf{k}_s, \mathbf{k}_i) = \begin{bmatrix} A_{11}(\mathbf{k}_s, \mathbf{k}_i) & A_{12}(\mathbf{k}_s, \mathbf{k}_i) \\ A_{21}(\mathbf{k}_s, \mathbf{k}_i) & A_{22}(\mathbf{k}_s, \mathbf{k}_i) \end{bmatrix} \tag{5}$$

Using the property of invariance of the scattering amplitude for horizontal and vertical shift of boundary, the matrix $\mathbf{A}$ is written as:

$$\mathbf{A}(\mathbf{k}_s, \mathbf{k}_i) = \int \mathbf{\Phi}(\mathbf{k}_s, \mathbf{k}_i; h(\mathbf{r}))\exp(-i(\mathbf{k}_s - \mathbf{k}_i)\cdot r + iQh(\mathbf{r}))d\mathbf{r} \tag{6}$$

Where Q is defined as $Q = -q_{ki} - q_{ks}$.

$\mathbf{\Phi}$ is an arbitrary functional of $h(\mathbf{r})$, which can be sought in the form of the integral-power series given by the following expression:

$$\begin{aligned}\mathbf{\Phi}(\mathbf{k}_s, \mathbf{k}_i; h(\mathbf{r})) = \mathbf{\Phi}_0(\mathbf{k}_s, \mathbf{k}_i) &+ \int \mathbf{\Phi}_1(\mathbf{k}_s, \mathbf{k}_i; \mathbf{k})H(\mathbf{k})\exp(+i\mathbf{k}.\mathbf{r})d\mathbf{k}/(2\pi)^2 \\ &+ \int \mathbf{\Phi}_2(\mathbf{k}_s, \mathbf{k}_i; \mathbf{k}_1, \mathbf{k}_2)H(\mathbf{k}_1)H(\mathbf{k}_2)\exp(+i(\mathbf{k}_1 + \mathbf{k}_2)\cdot\mathbf{r}) \\ &\quad d\mathbf{k}_1 d\mathbf{k}_2/(2\pi)^4 + \ldots\end{aligned} \tag{7}$$

Where $\mathbf{\Phi}_0(\mathbf{k}_s, \mathbf{k}_i)$ and $\{\mathbf{\Phi}_n(\mathbf{k}_s, \mathbf{k}_i; \mathbf{k}_1, \mathbf{k}_2)\}_{n\geq 1}$ are the coefficients of the power series respectively at the orders 0 and $n \geq 1$.

$H(\mathbf{k})$ is the Fourier transform of the roughness shape $h(\mathbf{r})$:

$$H(\mathbf{k}) = \int h(\mathbf{r}) \exp(-i\mathbf{k}.\mathbf{r}) d\mathbf{r} \tag{8}$$

For $n \geq 1$, the coefficient functions $\mathbf{\Phi}_n$ vanish when one of the arguments $\mathbf{k}_j$, for $j = 1 \ldots n$, becomes zero. In taking into account the symmetry of these coefficient functions, we can define new $\tilde{\mathbf{\Phi}}_n$ functions for $n \geq 1$:

$$\mathbf{\Phi_n}(\mathbf{k}_s, \mathbf{k}_i; \mathbf{k}_1, \ldots, \mathbf{k}_n) = \sum_{\beta_1,\ldots,\beta_n} k_{1\beta_1} \ldots k_{n\beta_n} \tilde{\mathbf{\Phi}}_{\mathbf{n}\beta_1,\ldots,\beta_n}(\mathbf{k}_s, \mathbf{k}_i; \mathbf{k}_1, \ldots, \mathbf{k}_n) \tag{9}$$

Where $\beta_j = (1, \ldots, n) = (x, y)$, $\mathbf{k}_j = k_{j_x}\mathbf{u}_x + k_{j_y}\mathbf{u}_y$.

The functions $\tilde{\mathbf{\Phi}}_\mathbf{n}$ are regular functions without singularities at $\mathbf{k}_j = 0$ for $j = 1, \ldots, n$.

We substitute (9) into (7), then we obtain the following expression:

$$\begin{aligned} & \mathbf{\Phi}(\mathbf{k}_s, \mathbf{k}_i; h(\mathbf{r})) \\ = \; & \mathbf{\Phi_0}(\mathbf{k}_s, \mathbf{k}_i) + \int \sum_\beta \tilde{\mathbf{\Phi}}_{\mathbf{1}\beta}(\mathbf{k}_s, \mathbf{k}_i; \mathbf{k}) k_\beta H(\mathbf{k}) \exp(+i\mathbf{k}\cdot\mathbf{r}) d\mathbf{k}/(2\pi)^2 \\ & + \int \sum_{\beta_1,\beta_2} \tilde{\mathbf{\Phi}}_{\mathbf{2}\beta_1,\beta_2}(\mathbf{k}_s, \mathbf{k}_i; \mathbf{k}_1, \mathbf{k}_2) k_{1\beta_1} k_{2\beta_2} H(\mathbf{k}_1) H(\mathbf{k}_2) \\ & \exp(+i(\mathbf{k}_1 + \mathbf{k}_2)\cdot\mathbf{r}) d\mathbf{k}_1 d\mathbf{k}_2/(2\pi)^4 + \ldots \end{aligned} \tag{10}$$

The functions $\tilde{\mathbf{\Phi}}_\mathbf{n}$ are bounded for all $\mathbf{k}_1, \ldots, \mathbf{k}_n$, then $\mathbf{A_n}$ is defined as $|\tilde{\mathbf{\Phi}}_\mathbf{n}| < \mathbf{A_n}$. And as we have:

$$\int k_{j_{\beta_j}} H(\mathbf{k}_j) \exp(+i\mathbf{k}_j\cdot\mathbf{r}) d\mathbf{k_j}/(2\pi)^2 = -i\nabla_{\beta_j} h(\mathbf{r}) \tag{11}$$

The successive terms of the expansion (10) are of order $|\nabla h|^n \mathbf{A_n}$. The expansion (10) can be considered as a surface slope expansion. If $|\nabla h| \ll 1$, we obtain a small-slope expansion. To determine the functions $\tilde{\mathbf{\Phi}}_\mathbf{n}$, Voronovich [16–18] proposed to identify the expression (10) with the small perturbation theory (SPT), if the common integral-power expansion of SA is known.

In the framework of the small perturbation theory, the scattering amplitude at order two is given by the following expression:

$$\begin{aligned} \mathbf{A}(\mathbf{k}_s, \mathbf{k}_i) \; = \; & (2\pi)^2 \mathbf{B}_0(\mathbf{k}_s, \mathbf{k}_i)\delta(\mathbf{k}_s - \mathbf{k}_i) + 2iq_{ki}\mathbf{B}_1(\mathbf{k}_s, \mathbf{k}_i) H(\mathbf{k}_s - \mathbf{k}_i) \\ & + q_{ki} \int \mathbf{B}_2(\mathbf{k}_s, \mathbf{k}_i; \mathbf{k}) H(\mathbf{k}_s - \mathbf{k}) H(\mathbf{k} - \mathbf{k}_i) d\mathbf{k} + \ldots \end{aligned} \tag{12}$$

Where $\mathbf{B}_0(\mathbf{k}_s, \mathbf{k}_i)$, $\mathbf{B}_1(\mathbf{k}_s, \mathbf{k}_i)$ and $\mathbf{B}_2(\mathbf{k}_s, \mathbf{k}_i; \mathbf{k})$ are respectively the scattering matrix of order 0,1 and 2. We can note that $\mathbf{B}_0(\mathbf{k}_s, \mathbf{k}_i)$ is the Fresnel reflection matrix in the specular direction and $\mathbf{B}_1(\mathbf{k}_s, \mathbf{k}_i)$ is the Bragg kernel. The calculation of $\mathbf{B}_2(\mathbf{k}_s, \mathbf{k}_i)$ does not present any great difficulties; we can find the expression of the small perturbation at order two in [17, 18, 24]. With the second-order solution, which is the lowest-order correction for the coherent reflection, the depolarization of the backscattered power is given. We can note that the second-order solution is needed to ensure energy conservation.

The functions $\tilde{\mathbf{\Phi}}_\mathbf{n}$ are determined after expanding the exponent of $\mathbf{A}(\mathbf{k}_s, \mathbf{k}_i)$ given by (6) in h, using the expression (10) and then comparing the result to the expansion (12). The expansion of the small-slope approximation at order 2 is then given by the following expression:

$$\begin{aligned}\mathbf{A}(\mathbf{k}_s, \mathbf{k}_i) &= \frac{2q_{ki}}{Q} \int \left\{ \mathbf{B}_1(\mathbf{k}_s, \mathbf{k}_i) - \frac{i}{4} \int \mathbf{M}(\mathbf{k}_s, \mathbf{k}_i; \mathbf{k}) H(\mathbf{k}) \right. \\ &\left. \exp(+i\mathbf{k}\cdot\mathbf{r}) d\mathbf{k}/(2\pi)^2 \right\} \exp(-i(\mathbf{k}_s - \mathbf{k}_i)\cdot\mathbf{k} + iQh(\mathbf{k}))d\mathbf{k}\end{aligned} \tag{13}$$

Where

$$\mathbf{M}(\mathbf{k}_s, \mathbf{k}_i; \mathbf{k}) = \mathbf{B}_2(\mathbf{k}_s, \mathbf{k}_i; \mathbf{k}_s - \mathbf{k}) + \mathbf{B}_2(\mathbf{k}_s, \mathbf{k}_i; \mathbf{k}_i + \mathbf{k}) + 2Q\mathbf{B}_1(\mathbf{k}_s, \mathbf{k}_i) \tag{14}$$

The term with $\mathbf{B}_1(\mathbf{k}_s, \mathbf{k}_i)$ constitutes the first order SSA, the term with the expression given by $-\frac{i}{4}\int \mathbf{M}(\mathbf{k}_s, \mathbf{k}_i; \mathbf{k}) H(\mathbf{k}) \exp(+i\mathbf{k}\cdot\mathbf{r}) d\mathbf{k}/(2\pi)^2$ is the second-order SSA.

It is interesting to note, from the expressions (13) and (14), that the SSA gives the co- and cross-polarized contributions to the scattered field in the incident plane and out of the incident plane. We know that depolarization will occur for an arbitrary rough surface whose height is a function of both x and y.

According to simple single theory (KA for example), there is no depolarization for the coherent field in the case of perfectly conducting surfaces. For the incoherent or diffuse field, no depolarization is predicted within the azimuthal plane for perfectly conducting surfaces and there is depolarization for scattering outside this plane for perfectly or dielectric surfaces. Kirchhoff theory predicts depolarization for the backscattering direction when the surface is imperfectly conducting. But in the high frequency limit of Kirchhoff theory, we have no depolarization within the backscattered direction for surface of finite conductivity.

But experiments have contradicted these results; significant depolarization was measured within the azimuthal plane for light

incident upon gold or silver films. Therefore the SSA is more reliable than KA or SPM. Another theoretical point is noticeable in the small-slope approximation: the theory is applicable to randomly rough surfaces with Gaussian and non-Gaussian correlation functions without leading to reductions in the regimes of validity of the SSA theory. That is not the case for the KA theory, for example when high frequency roughness is present in surfaces with ocean spectrum or exponential correlation functions. The formulation of Kirchhoff theory for non-perfectly conducting surfaces is tedious because of the local surface fields, and numerical evaluation is required contrary to the SSA formulation.

For a randomly rough surface with a root mean height δ and a correlation length ℓ, the validity domain of the small-slope approximation is given by the expression:

$$\delta/\ell < \mathrm{Min}(q_i/k_i, q_d/k_d) = \mathrm{Min}(1/\tan\theta_i, 1/\tan\theta_d)$$

The previous expression is independent of the wavelength. But the validity of the SSA method must be checked at grazing angles.

2.2. Scattered Fields and Scattering Cross-Sections

The scattering properties are analyzed in the far-field zone. Using the stationary approximation in expression (3), we show that the asymptotic scattered field at the distance R is given:

$$\mathbf{E}^s \approx -iq_{ks} \sum_{\alpha_s=1,2} A_{\alpha_s\alpha_i}(\mathbf{k}_s, \mathbf{k}_i)\mathbf{e}^s_{\alpha_s}(\mathbf{k}_s) \exp(iK_1R)/(2\pi R) \tag{15}$$

The far-field scattering matrix $\mathbf{S}$ is defined by the expression $\mathbf{E^s} = \mathbf{SE^i}$, which leads to:

$$\mathbf{S}(\mathbf{k}_s, \mathbf{k}_i) \approx -iq_{ks}\mathbf{A}(\mathbf{k}_s, \mathbf{k}_i) \exp(iK_1R)/(2\pi R) \tag{16}$$

For a deterministic scattering process, the scattering cross-section (radar or laser cross-section) is defined as follows:

$$\boldsymbol{\sigma}(\mathbf{k}_s, \mathbf{k}_i) = 4\pi R^2 |\mathbf{S}(\mathbf{k}_s, \mathbf{k}_i)|^2 \tag{17}$$

The scattering from a randomly rough surface is a stochastic process, since statistical methods are used to describe surface properties and the field will be a random function characterized by statistical parameters. The scattering cross-section of a randomly rough surface has then to be defined in terms of the average scattered intensity.

$$\boldsymbol{\sigma}(\mathbf{k}_s, \mathbf{k}_i) = 4\pi R^2 \left\langle |\mathbf{S}(\mathbf{k}_s, \mathbf{k}_i)|^2 \right\rangle \tag{18}$$

The brackets $< \cdot >$ denote the ensemble average or spatial average of a random quantity. We must note that an important assumption in the theory of wave scattering from randomly rough surfaces is that the surface we consider is ergodic, i.e., any statistical average taken over several different parts of one surface realization is the same as an average over many surface realizations (ensemble realization). We use the notation of brackets to denote both spatial and ensemble averaging. We determine the mean amplitude and intensity of the scattered field. The mean amplitude gives information on the coherent component of the scattered field, the mean intensity on the diffuse component of the field. The total field is given by the sum of the coherent and diffuse (incoherent) fields. The total scattering cross-section (laser cross-section or radar cross-section) $\boldsymbol{\sigma}$ is decomposed into a coherent component $\boldsymbol{\sigma}_C$ and an incoherent component $\boldsymbol{\sigma}_I$ defined respectively by:

$$\boldsymbol{\sigma}_C(\mathbf{k}_s, \mathbf{k}_i) = 4\pi R^2 \left| \left\langle \mathbf{S}(\mathbf{k}_s, \mathbf{k}_i) \right\rangle \right|^2 \tag{19}$$

$$\boldsymbol{\sigma}_I(\mathbf{k}_s, \mathbf{k}_i) = 4\pi R^2 \left\{ \left\langle |\mathbf{S}(\mathbf{k}_s, \mathbf{k}_i)|^2 \right\rangle - \left| \left\langle |\mathbf{S}(\mathbf{k}_s, \mathbf{k}_i)| \right\rangle \right|^2 \right\} \tag{20}$$

In the optical region, where materials have finite conductivity and the surface irregularities have a wide range in size relative to the wavelength, one way to determine reflectance is to define the bi-directional reflectance distribution function (BRDF). For an element of surface A illuminated by an incident electromagnetic wave, we have the relation between the scattering cross-section (laser cross-section) and the BRDF

$$\boldsymbol{\sigma}(\mathbf{k}_s, \mathbf{k}_i) = 4\pi A \cos(\theta_i) \cos(\theta_s) \mathbf{BRDF}(\mathbf{k}_s, \mathbf{k}_i) \tag{21}$$

The coherent and incoherent components of the scattering cross-section are given using the second-order small-slope approximation (13) and (14). We assume that the distribution of the randomly rough surface heights is described by a zero-mean Gaussian process with any correlation function $C(\boldsymbol{\rho})$. The coherent component is obtained by directly averaging (13) and (14) over the surface heights. In the framework of the small-slope approximation of order two, the mean scattering amplitude is given by the following expression:

$$\langle \mathbf{A}(\mathbf{k}_s, \mathbf{k}_i) \rangle = \frac{2q_{ki}}{Q} \chi_1(Q) \int \{\mathbf{B_1}(\mathbf{k}_s, \mathbf{k}_i) - \mathbf{F}(\mathbf{k}_s, \mathbf{k}_i; \mathbf{0})\} \exp(-i(\mathbf{k}_s - \mathbf{k}_i)\cdot\mathbf{r}) d\mathbf{r} \tag{22}$$

Where

$$\mathbf{F}(\mathbf{k}_s, \mathbf{k}_i; \mathbf{r}) = -\frac{Q}{4} \int \mathbf{M}(\mathbf{k}_s, \mathbf{k}_i; \mathbf{k}) S(\mathbf{k}) \exp(+i\mathbf{k} \cdot \mathbf{r}) d\mathbf{k}/(2\pi)^2 \quad (23)$$

Where $S(\mathbf{k})$ is the power spectral density (PSD) of the randomly rough surface and $\chi_1(Q)$ is the one-dimensional characteristic function of the randomly rough surface. This characteristic function is the Fourier transform of the probability density function. For a random rough surface with a Gaussian probability density function, the characteristic function $\chi_1(Q)$ is given by:

$$\chi_1(Q) = \exp(-Q^2 C(0)/2) \quad (24)$$

The coherent scattering cross-section is given by the following expression taking into account the second order of the small-slope approximation:

$$\begin{aligned} \boldsymbol{\sigma}_C(\mathbf{k}_s, \mathbf{k}_i) &= \left(\frac{2 q_{ki} q_{ks}}{Q\sqrt{\pi}} \right)^2 \chi_1^2(Q) |\mathbf{B_1}(\mathbf{k}_s, \mathbf{k}_i) - \mathbf{F}(\mathbf{k}_s, \mathbf{k}_i; \mathbf{0})|^2 \\ & \iint \exp(-i(\mathbf{k}_s - \mathbf{k}_i) \cdot (\mathbf{r} - \mathbf{r}')) d\mathbf{r} d\mathbf{r}' \end{aligned} \quad (25)$$

With $\mathbf{r} = (x, y)$ and $\mathbf{r}' = (x', y')$, we can write the previous integral term as follows:

$$\begin{aligned} I_S &= \int_{\mathbf{r}} \int_{\mathbf{r}'} e^{-i(\mathbf{k}_s - \mathbf{k}_i) \cdot (\mathbf{r} - \mathbf{r}')} d\mathbf{r}' d\mathbf{r} \\ &= \int_x \int_y \int_{x'} \int_{y'} e^{-i[(k_{s_x} - k_{i_x}).(x - x') + (k_{s_y} - k_{i_y}).(y - y')]} dx' dy' dx dy \end{aligned} \quad (26)$$

Where the expression is determined by integrating upon the illuminated portion of the surface. For a rectangular surface $[L_x; L_y]$, I_S is given by :

$$I_S = \int_{-L_x}^{+L_x} \int_{-L_y}^{+L_y} (L_x - |x|) (L_y - |y|) e^{-i[(k_{s_x} - k_{i_x}).x + (k_{s_y} - k_{i_y}).y]} dx dy \quad (27)$$

Then

$$I_S = (L_x L_y)^2 \mathrm{sinc}^2 \left[(k_{s_x} - k_{i_x}) L_x/2 \right] \mathrm{sinc}^2 \left[(k_{s_y} - k_{i_y}) L_y/2 \right] \quad (28)$$

Where $\mathrm{sinc}(x) = \sin(x)/x$. The function $p_S(x, y) = (L_x - |x|)(L_y - |y|)$ is the auto-correlation function of the considered rectangular domain.

The triangular case can be treated by calculating its auto-correlation function. For a rectangular domain $\lfloor L_x; L_y \rfloor$, the coherent scattering cross-section is given by:

$$\boldsymbol{\sigma}_C(\mathbf{k}_s, \mathbf{k}_i) = \left(\frac{2q_{ki}q_{ks}}{Q\sqrt{\pi}}\right)^2 \chi_1^2(Q)(L_xL_y)^2 |\mathbf{B}_1(\mathbf{k}_s, \mathbf{k}_i) - \mathbf{F}(\mathbf{k}_s, \mathbf{k}_i; \vec{0})|^2 I_S \tag{29}$$

With

$$I_S = (L_xL_y)^2 \mathrm{sinc}^2\left[(k_{sx} - k_{ix})L_x/2\right] \mathrm{sinc}^2\left[(k_{sy} - k_{iy})L_y/2\right]$$

The incoherent (or diffuse) component of the scattering cross-section is obtained by firstly averaging the intensity of (13) over the surface heights, and then subtracting the coherent component given by (25) to the total scattering cross-section. We can show that the total scattering cross-section is given by the following expression:

$$\begin{aligned} \boldsymbol{\sigma}(\mathbf{k}_s, \mathbf{k}_i) \;=\; & \left(\frac{2q_{ki}q_{ks}}{Q\sqrt{\pi}}\right)^2 \iint \chi_2(Q, -Q, \mathbf{r} - \mathbf{r}') \\ & \Big\{\Big(\mathbf{B}_1(\mathbf{k}_s, \mathbf{k}_i) + \mathbf{F}(\mathbf{k}_s, \mathbf{k}_i; \mathbf{r} - \mathbf{r}') - \mathbf{F}(\mathbf{k}_s, \mathbf{k}_i; \mathbf{0})\Big) \\ & \cdot\Big(\mathbf{B}_1(\mathbf{k}_s, \mathbf{k}_i) + \mathbf{F}(\mathbf{k}_d, \mathbf{k}_i; \mathbf{r}' - \mathbf{r}) - \mathbf{F}(\mathbf{k}_s, \mathbf{k}_i; \mathbf{0})\Big)^* \\ & + \mathbf{G}(\mathbf{k}_s, \mathbf{k}_i; \mathbf{r} - \mathbf{r}')\Big\}\, e^{-i(\mathbf{k}_s - \mathbf{k}_i)\cdot(\mathbf{r} - \mathbf{r}')} d\mathbf{r}' d\mathbf{r} \end{aligned} \tag{30}$$

Since:

$$\boldsymbol{\sigma}_{\mathbf{I}}(\mathbf{k}_s, \mathbf{k}_i) = \boldsymbol{\sigma}(\mathbf{k}_s, \mathbf{k}_i) - \boldsymbol{\sigma}_{\boldsymbol{C}}(\mathbf{k}_s, \mathbf{k}_i) \tag{31}$$

The incoherent scattering cross-section is given by:

$$\begin{aligned} \boldsymbol{\sigma}_{\mathbf{I}}(\mathbf{k}_s, \mathbf{k}_i) \;=\; & \left(\frac{2q_{ki}q_{ks}}{Q\sqrt{\pi}}\right)^2 \iint \mathbf{R}(\mathbf{k}_s, \mathbf{k}_i; \mathbf{r}, \mathbf{r}') \\ & \exp(-i(\mathbf{k}_s - \mathbf{k}_i)\cdot(\mathbf{r} - \mathbf{r}'))d\mathbf{r}d\mathbf{r}' \end{aligned} \tag{32}$$

Where

$$\begin{aligned} & \mathbf{R}(\mathbf{k}_s, \mathbf{k}_i; \mathbf{r}, \mathbf{r}') = \chi_2(Q, -Q, \mathbf{r} - \mathbf{r}') \\ & \Big\{\Big(\mathbf{B}_1(\mathbf{k}_s, \mathbf{k}_i) + \mathbf{F}(\mathbf{k}_s, \mathbf{k}_i; \mathbf{r} - \mathbf{r}') - \mathbf{F}(\mathbf{k}_s, \mathbf{k}_i; \mathbf{0})\Big) \\ & \Big(\mathbf{B}_1(\mathbf{k}_s, \mathbf{k}_i) + \mathbf{F}(\mathbf{k}_s, \mathbf{k}_i; \mathbf{r}' - \mathbf{r}) - \mathbf{F}(\mathbf{k}_s, \mathbf{k}_i; \mathbf{0})\Big)^* \\ & + \mathbf{G}(\mathbf{k}_s, \mathbf{k}_i; \mathbf{r}' - \mathbf{r})\Big\} - \chi_1^2(Q)|\mathbf{B}_1(\mathbf{k}_s, \mathbf{k}_i) - \mathbf{F}(\mathbf{k}_s, \mathbf{k}_i; \mathbf{0})|^2 \end{aligned} \tag{33}$$

$\chi_2(Q,-Q,\boldsymbol{\rho})$ is the two-dimensional characteristic function and $\mathbf{G}$ is given by:

$$\mathbf{G}(\mathbf{k}_s,\mathbf{k}_i;\mathbf{r}) = \frac{1}{16}\int |\mathbf{M}(\mathbf{k}_s,\mathbf{k}_i;\mathbf{k})|^2 S(\mathbf{k})\exp(+i\mathbf{k}\cdot\mathbf{r})d\mathbf{k}/(2\pi)^2 \quad (34)$$

For a randomly rough surface described by a Gaussian density probability function and any correlation function $C(\boldsymbol{\rho})$, the two-dimensional characteristic function is given by:

$$\chi_2(Q,-Q,\boldsymbol{\rho}) = \exp\Big(-Q^2(C(\mathbf{0})-C(\boldsymbol{\rho}))\Big) \quad (35)$$

We must note that the product of the matrices $(\mathbf{X})\cdot(\mathbf{Y})^*$ in the expressions (30) and (33) is defined as a product term by term between the elements of the matrix $\mathbf{X}$ and the complex conjugate elements of the matrix $\mathbf{Y}$.

If the illuminated surface is a rectangular surface with the following dimensions $\lfloor \mathbf{L}_x;\mathbf{L}_y \rfloor$, the integral defining the incoherent scattering cross-section is given by:

$$\begin{aligned}\boldsymbol{\sigma}_I(\mathbf{k}_s,\mathbf{k}_i) \;=\; & \left(\frac{2q_{ki}q_{ki}}{Q\sqrt{\pi}}\right)^2 \int_{-L_x}^{L_x}\int_{-L_y}^{L_y}(L_x-|x|)(L_y-|y|)\Big(\chi_2(Q,-Q,\mathbf{r}) \\ & \Big\{\Big(\mathbf{B}_1(\mathbf{k}_s,\mathbf{k}_i)+\mathbf{F}(\mathbf{k}_s,\mathbf{k}_i;\mathbf{r})-\mathbf{F}(\mathbf{k}_d,\mathbf{k}_i;\mathbf{0})\Big) \\ & \cdot\Big(\mathbf{B}_1(\mathbf{k}_s,\mathbf{k}_i)+\mathbf{F}(\mathbf{k}_d,\mathbf{k}_i;-\mathbf{r})-\mathbf{F}(\mathbf{k}_d,\mathbf{k}_i;\mathbf{0})\Big)^* \\ & +\mathbf{G}(\mathbf{k}_s,\mathbf{k}_i;\mathbf{r})\} - \chi_1^2(Q)|\mathbf{B}_1(\mathbf{k}_s,\mathbf{k}_i)-\mathbf{F}(\mathbf{k}_s,\mathbf{k}_i;\mathbf{0})|^2\Big) \\ & e^{-i(\mathbf{k}_s-\mathbf{k}_i)\cdot\mathbf{r}}dxdy \end{aligned} \quad (36)$$

With $\mathbf{r}=(x,y)$.

With the expressions (29) and (36) we can numerically calculate the coherent and the incoherent scattering cross-sections of a random rough surface with a Gaussian height probability distribution and with any correlation function (or power spectral density function). The power spectral density function $S(\mathbf{k})$ is usually defined as the Fourier transform of the correlation function $C(\boldsymbol{\rho})$. We can use these two alternative descriptions of a randomly rough surface as data for our analytical expressions of the scattering cross-sections.

For a rectangular surface defined on the spatial domain $x \in [-L_x/2;+L_x/2]$ and $y \in [-L_y/2;+L_y/2]$, the scattering cross-section is obtained by calculating (36) in the domain $x \in [-L_x;+L_x]$ and $y \in$

$[-L_y; +L_y]$. The integrand contains the spatial functions $\chi_2(Q, -Q, \mathbf{r})$, $\mathbf{F}(\mathbf{k}_s, \mathbf{k}_i; \mathbf{r})$, and $\mathbf{G}(\mathbf{k}_s, \mathbf{k}_i; \mathbf{r})$. But we can note that these functions depend on the wave numbers $\mathbf{k}_s$ and $\mathbf{k}_i$ defining the scattering and incident directions: this integral (36) is not a simple Fourier transform. (36) is calculated by a numerical integration. The functions $\mathbf{F}(\mathbf{k}_s, \mathbf{k}_i; \mathbf{r})$ and $\mathbf{G}(\mathbf{k}_s, \mathbf{k}_i; \mathbf{r})$ are calculated by an inverse Fourier transform in taking into account the functions $\mathbf{M}(\mathbf{k}_s, \mathbf{k}_i; \mathbf{k})$ and $S(\mathbf{k})$.

The inverse Fourier transform is calculated in a frequency domain defined owing to the characteristics of the integrated dual spatial domain. The functions $\mathbf{M}(\mathbf{k}_s, \mathbf{k}_i; \mathbf{k})$ and $S(\mathbf{k})$ are calculated in this frequency domain. We must note that the function $\mathbf{M}(\mathbf{k}_s, \mathbf{k}_i; \mathbf{k})$ is calculated with the coefficients $\mathbf{B}_2(\mathbf{k}_s, \mathbf{k}_i; \mathbf{k}_s - \mathbf{k})$, $\mathbf{B}_2(\mathbf{k}_s, \mathbf{k}_i; \mathbf{k}_s + \mathbf{k})$, and $\mathbf{B}_1(\mathbf{k}_s, \mathbf{k}_i)$.

The calculation of the coherent component of the scattering cross-section does not present any real difficulty. The characteristic function $\chi_1(Q)$ is calculated from the value at the origin of the correlation function. From $\mathbf{F}(\mathbf{k}_s, \mathbf{k}_i; \mathbf{r})$, we have easily the value of $\mathbf{F}(\mathbf{k}_s, \mathbf{k}_i; \mathbf{0})$.

3. NUMERICAL EXAMPLES AND COMPARISON WITH EXPERIMENTAL DATA

Predictions of the scattering model described in Section 2 are compared with a variety of experimental data. Illustrative examples are considered in this section, where the incoherent diffuse scattering cross-sections for two-dimensional dielectric and metallic surfaces are computed and compared with experimental data. In this paper, we consider:

(i) conducting homogeneous isotropic Gaussian rough surfaces,

(ii) dielectric homogeneous isotropic Gaussian rough surfaces,

(iii) dielectric homogeneous isotropic rough surfaces with Gaussian surface height distribution and Lorentzian correlation function,

(iv) conducting non-isotropic rough surfaces, the surface height distribution is Gaussian and the correlation function or the power spectral density function is non-isotropic and non-Gaussian.

3.1. Conducting Isotropic Gaussian Surfaces: Numerical Calculations and Comparison with Experimental Data

The small-slope approximation method is compared with experimental data obtained by O'Donnel and Mendez [25] for scattering by a gold rough surface at $10.6\,\mu$m. We can find the histogram of height distribution and the auto-correlation function given by O'Donnel and

Mendez in Figure 2. This figure corresponds to the Figures 3 and 4 of the paper [25]. The histogram of height distribution and the auto-correlation function are obtained with a surface profilometer. The surface is assumed to be isotropic. Measurements suggest that the height probability density function and the correlation function are Gaussian. The statistical data are the following ones:

$$\begin{aligned} \text{RMS height } \delta &= 2.27\,\mu\text{m} \\ \text{Correlation length } \ell &= 20.9\,\mu\text{m}. \end{aligned}$$

For each angle of incidence, measurements and calculations are made with H-polarization incident and H-polarization collected ('HH' scattering) and V-polarization incident and V-polarization collected ('VV' scattering). The measured incoherent HH-polarized components for incident angles $\theta_i = 20^\circ$ and $\theta_i = 70^\circ$ in the azimuthal plane $\phi_i = 0^\circ$ are given in Figure 3 and compared with the incoherent components calculated by the second-order SSA method. A_p is the projection of the illuminated surface area (radar footprint) onto the reference plane. We normalize the scattering cross-section by dividing it by A_p. The same definition is applied to the measurements and the numerical simulations. The characteristics of the measured surface verify $K\delta = 1.34$, $\delta/\ell \approx 0.108$, and $K\ell = 12.38$ at the considered wavelength $10.6\,\mu$m. This case may be considered to be in the intermediate rough surface range with small slope. For the numerical simulation of the incoherent intensity with the small-slope approximation, we consider the index of refraction of gold at $10.6\,\mu$m. The small-slope approximation is in good agreement with the experimental data. The small deviations between the SSA and the experimental data are due to the fact that it is assumed the surface height distribution function and the surface height auto-correlation function are Gaussian. But the histogram of the height distribution and the true auto-correlation function, as we can see in the Figure 2, are not exactly Gaussian. The auto-correlation function is no more Gaussian for large arguments. The SSA is also shown to agree with the full-wave method taking into account the height/slope correlation [26].

3.2. Dielectric Isotropic Gaussian Surfaces: Numerical Calculations and Comparison with Experimental Data

3.2.1. Experimental Data Obtained by Chaikina et al. [27]

We also carry out a careful comparison between the second-order small-slope approximation and experimental measurements given by Chaikina et al. [27]. Chaikina et al. consider measurements of light

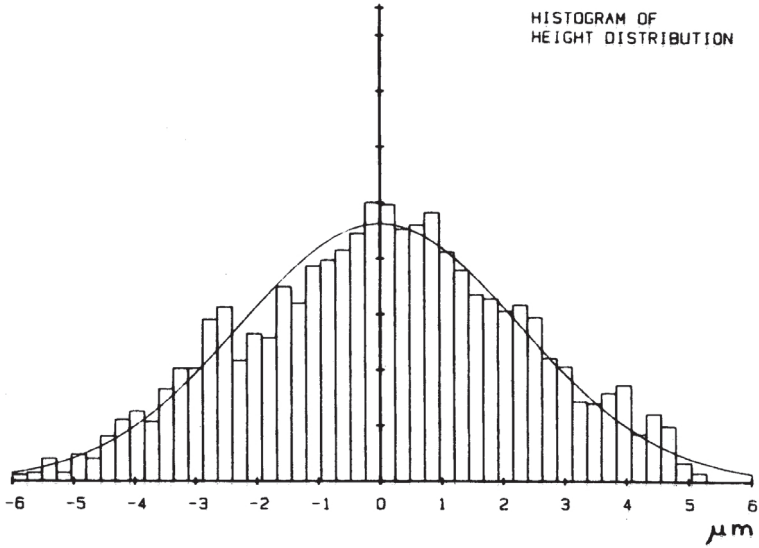

Fig. 3. Histogram of surface height data of diffuser #80 in comparison with a Gaussian distribution of the same variance. This was produced from 1000 measurements taken with a surface profilometer.

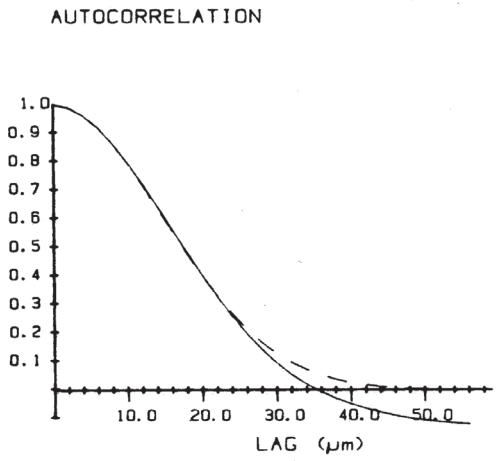

Fig. 4. Autocorrelation function (solid line) of profilometer surface height data of diffuser #80 as compared with a Gaussian function (dashed line).

Figure 2. Statistical descriptions of the surface given by O'Donnell et Mendez [25].

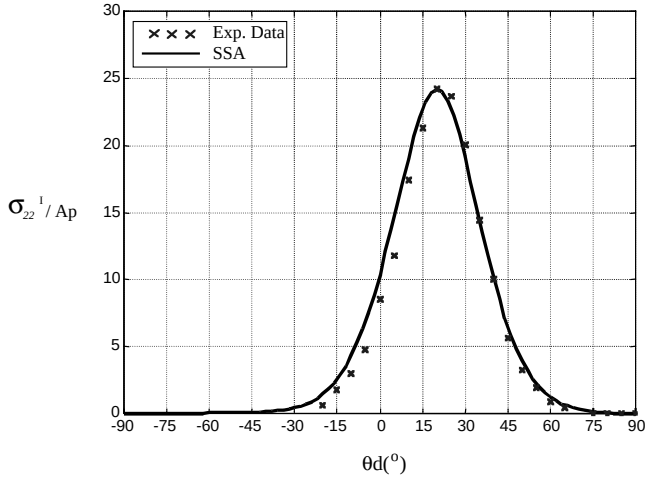

(a) Incoherent component for polarization $\alpha_d\,\alpha_i$ =22 (HH), the incident angle is $\theta_i = 20^\circ$.

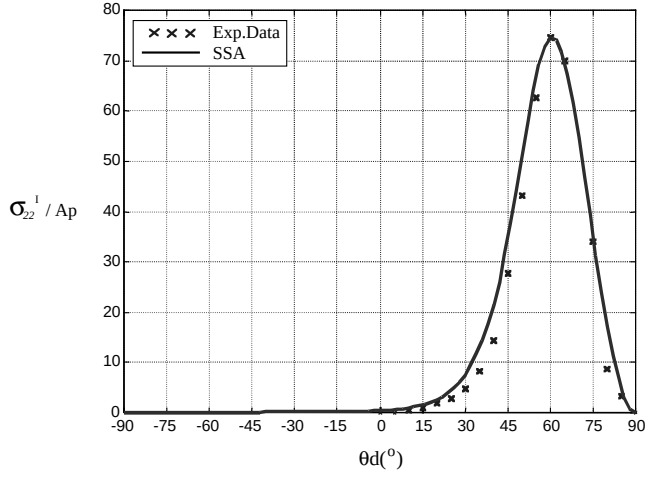

(b) Incoherent component for polarization $\alpha_d\,\alpha_i$ =22 (HH), the incident angle is $\theta_i = 70^\circ$.

Figure 3. Comparison of the experimental data obtained by O'Donnell et Mendez [25], for horizontal polarization ($\alpha_d\alpha_i = 22$) at $\lambda = 10.6\,\mu$m, with the second-order small-slope approximation.

scattering at 0.808 μm from a rough thin film deposited upon a glass of refraction index $N = 1.69$. The index of refraction of the film is $N = 1.63$. The sample is assumed to be Gaussian, homogeneous and isotropic. The surface height distribution function and the surface height autocorrelation function are assumed to be Gaussian functions. The statistical characteristics of the rough film are the following ones: $\delta = 0.37\,\mu$m and $\ell = 3.1\,\mu$m. The RMS surface roughness δ and the correlation length ℓ are calculated assuming a Gaussian surface height probability density and a Gaussian correlation function. The Figure 4 gives the measured incoherent components for the polarization VV ($\alpha_d\alpha_i = 11$) and polarization HH ($\alpha_d\alpha_i = 22$) in the azimuthal plane $\phi_i = 0°$. The angle of incidence is $\theta_i = 20°$. The experimental data are compared with the second-order small approximation. A_p is the projection of the illuminated surface area (radar footprint) onto the reference plane. In Figure 4, $K\delta = 2.877$, $\delta/\ell = 0.1$, and $K\ell = 24.10$, this surface is considered to be in the intermediate rough surface range. Similar to the case in Figure 3, the small-slope approximation is in good agreement with the experimental measurements.

3.2.2. Experimental Data Obtained by O. Calvo-Perez [28]

The main progress is the development of the vector wave case of the second-order small-slope approximation method for dielectric two-dimensional surfaces. To compare experimental data with our numerical simulations, we choose two-dimensional samples realized by O. Calvo-Perez. An important feature of the work of O. Calvo-Perez was that the surface samples were well characterized, with Gaussian statistics for the surface height and the correlation function. Since the statistics of the surface were known, a critical comparison between experiment and our numerical theory could be made with confidence. The results we present in this part are intended to supplement those already reported with the aim of providing a reliable body of experiment data for comparison with model prediction.

The samples were fabricated to achieve Gaussian dielectric surfaces, which can be compared with scattering models at 632.8 nm. To obtain experimental data, three phases are necessary: surface preparation, surface characterization and measurements of the intensity of laser light scattered from the prepared surface. O. Calvo-Perez carried out experiments using surfaces manufactured by exposure of photoresist to speckle pattern. The statistics of speckle pattern are well known and Gaussian. Master surfaces were produced by exposing a thick layer of photoresist to statistically independent laser speckle patterns. Thus, surface samples with both a Gaussian height distribution function and correlation function were fabricated

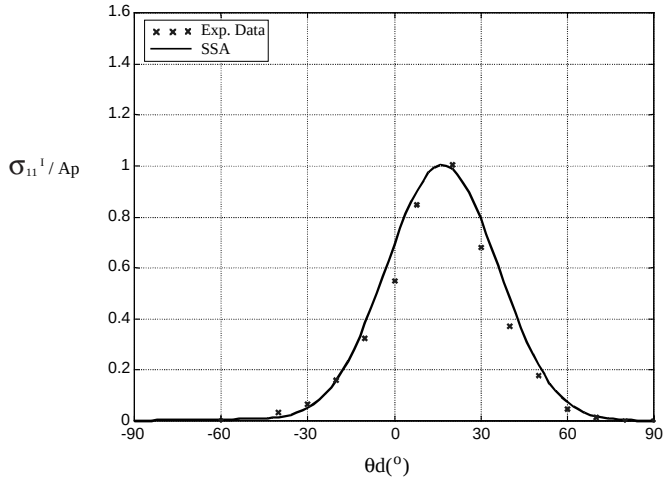

(a) Incoherent component for polarization $\alpha_d\,\alpha_i$ =11 (VV), the incident angle is $\theta i = 20^{\circ}$.

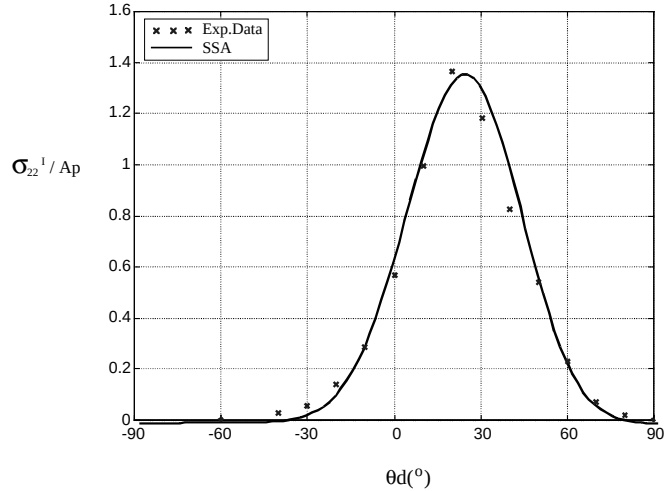

(b) Incoherent component for polarization $\alpha_d\,\alpha_i$ =22 (HH), the incident angle is $\theta i = 20^{\circ}$.

Figure 4. Comparison of the experimental data obtained by Chaikina et al. [27], for HH- and VV-polarizations at $\lambda = 0.808\,\mu$m with the second-order small-slope approximation.

so that their surface statistics were described by a RMS height and a correlation length. The sample materials consist of dielectric resin on BK7 glass substrate to avoid deterioration of the resin. The refraction index of the resin is $n = 1.62 + i0.001$, it is an almost lossless dielectric. This index was characterized by ellipsometry. The index of the BK7 glass is almost identical. The depth of the resin is about $10\,\mu$m.

The second phase is the characterization of the randomly rough surface. We know that the horizontal resolution of a profilometer is limited to about $0.4\,\mu$m because of the finite size of the stylus and the contact of the stylus can deteriorate the surface of the resin. A further problem arises when surface statistics are deduced from measurement made on one-dimensional profiles. Since the surface is two-dimensional, information is necessarily lost when profiles are considered. This often leads to an underestimate of surface properties such as RMS height. To overcome these difficulties, several square pieces of the rough surface were examined with an atomic force microscope (AFM). The vertical resolution of the AFM is 0.1 nm; the horizontal resolution is less than 10 nm. These resolutions are very much smaller than the incident wavelength. The AFM can be used in contact mode or in non-contact mode. The non-contact mode was chosen to avoid deteriorating of the photoresist sample. Many limited surface structure measurements were undertaken. Several $80\,\mu$m square sections were analyzed. Analysis of the AFM pictures showed that the surface was composed of smooth regions. This method of surface measurement is ideally suited to the digitization of the surface profile and the storage of this information for data processing. Statistical surface properties such as the root mean square height of the surface and the correlation length are easily extracted from the data. For the sample, the extracted root mean square height is $\delta = 0.223\,\mu$m and the extracted correlation length is $\ell = 1.42\,\mu$m. We can note that the precision of these values is about 5%.

The angular distribution of the scattered light was measured at one wavelength. The source is a helium-neon laser 632.8 nm, the beam is polarized: light, which is p-polarized has its electric field vector in the plane of incidence (V polarization in radar terminology) and s-polarized light is orthogonal to the plane of incidence (H polarization in radar terminology). The detector is mounted on a computer-controlled mount to allow precise incident and scattering directions. The principal noise sources were reflections from the interface BK7/air. To avoid these unwanted reflections upon the interface of the sample, an absorbing glass is placed behind the BK7 substrate. An accuracy of better than 10% is expected for the measure of the scattering cross-sections except in the specular direction where we can find the principal

noise sources, which are the reflections at the different interfaces of the sample.

Laser scattering measurements of the Gaussian sample were performed at a variety of incident angles, in the plane of incidence. Measurements were made with both V- and H-polarized light. Incoherent bistatic cross-section predictions for incidence angles of 20°, 35°, 45°, 55°, 70° and a wavelength of 632.8 nm are illustrated in Figures 5(a), (b), 6(a), (b), 7(a), (b), 8(a), (b) and 9(a), (b) along with corresponding experimental data in HH- and VV-polarization. The incoherent bistatic cross-section is given by the Differential Reflection Coefficient (DRC), which is related to the definition of the BRDF by the following expression:

$$\mathbf{DRC} = \mathbf{BRDF}\cos(\theta_s) \tag{37}$$

Where θ_s is the scattering angle.

The model parameters employed for the SSA predictions are the following ones: $\lambda = 632.8\,\text{nm}$, the statistical characteristics of the dielectric rough surface are assumed to be Gaussian with $\delta = 0.223\,\mu\text{m}$, $\ell = 1.42\,\mu\text{m}$, $K\ell = 14.1$, $K\delta = 2.21$, $\delta/\ell = 0.157$. The randomly rough surface is assumed to be a rough interface between two 2-dimensional dielectric half-spaces, air and resin of refraction index $n = 1.62 + i0.001$.

Overall, the agreement between experiment and theory is observed to be very good, especially given that the absolute scattering coefficients are compared with no adjustable parameters. Illustrative of the accuracy of reflectance predictions resulting from the small-slope approximation are the experimental data and SSA predictions plotted in Figures 5, 6, 7, 8 and 9. We find an excellent agreement between model predictions and experimental data, especially for the angle of incidence 55°. It is interesting to observe a minimum for vertical polarization similar to the Brewster angle for a smooth uniform surface. In the case of a smooth surface, there is no reflected power at the Brewster angle. By analogy with reflection from a planar surface, using a value of $n = 1.62$ for the refractive index of the almost lossless dielectric gives a Brewster angle of ≈58°. It is noteworthy that the dramatically different cross-section distribution at an incident angle of 55° for the VV-polarization, which results from the "Brewster angle" is very correctly predicted by the second-order small-slope approximation and the comparison with experimental data in the plane-of-incidence is excellent. A phenomenon of minimum of reflected power similar to the Brewster angle occurs for randomly rough surface considering single scattering to be the dominant mechanism. The predicted VV-polarized level of the forward scattering peaks is just slightly lower than the experimental data for incidence of 20° and 45°. For incidence

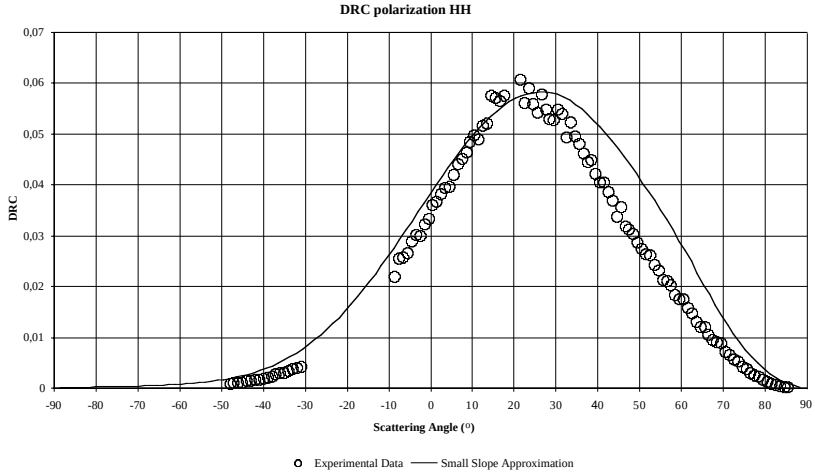

Figure 5a. Comparison of experimental data with the second-order small-slope approximation. 20° incident angle. Polarization HH, plane-of-incidence, bistatic, laser scattering data ($\lambda = 632.8\,\text{nm}$, $n = 1.62 + i0.001$, $\delta = 0.223\,\mu\text{m}$, $\ell = 1.42\,\mu\text{m}$).

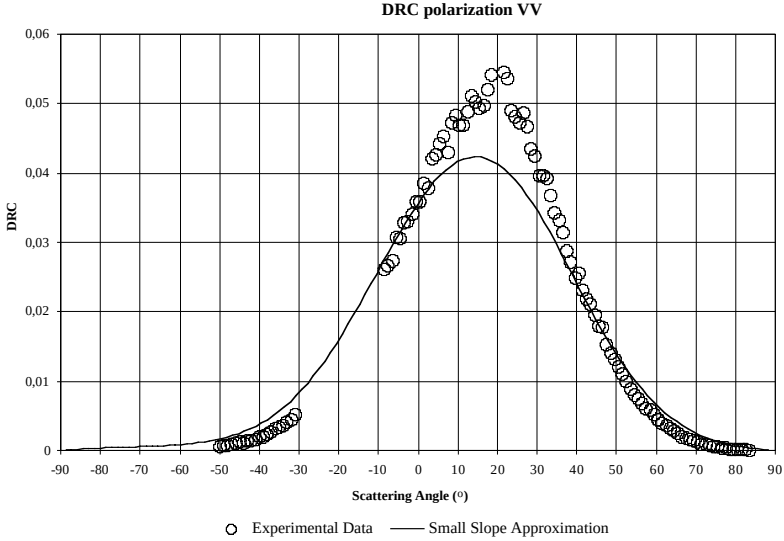

Figure 5b. Comparison of experimental data with the second-order small-slope approximation. 20° incident angle. Polarization VV, plane-of-incidence, bistatic, laser scattering data ($\lambda = 632.8\,\text{nm}$, $n = 1.62 + i0.001$, $\delta = 0.223\,\mu\text{m}$, $\ell = 1.42\,\mu\text{m}$).

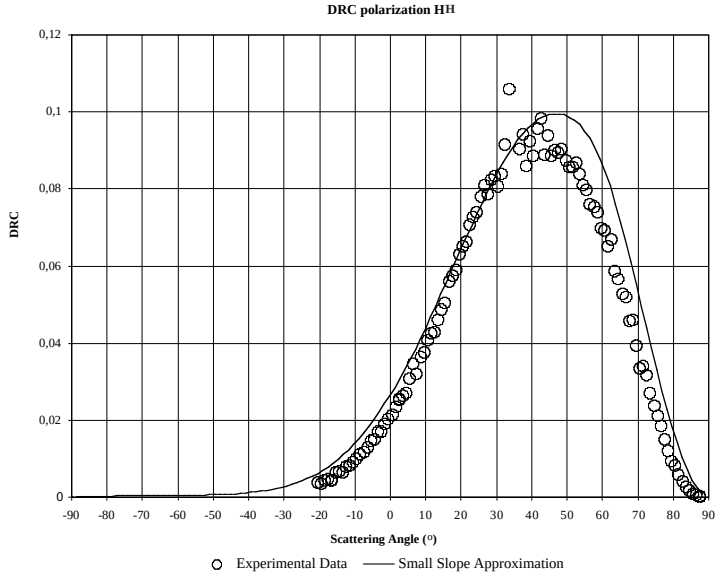

Figure 6a. Comparison of experimental data with the second-order small-slope approximation. 35° incident angle. Polarization HH, plane-of-incidence, bistatic, laser scattering data ($\lambda = 632.8\,\mathrm{nm}$, $n = 1.62 + i0.001$, $\delta = 0.223\,\mu\mathrm{m}$, $\ell = 1.42\,\mu\mathrm{m}$).

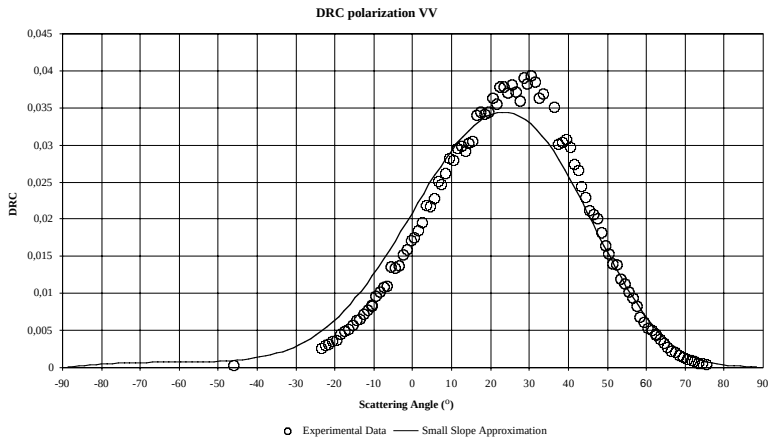

Figure 6b. Comparison of experimental data with the second-order small-slope approximation. 35° incident angle. Polarization VV, plane-of-incidence, bistatic, laser scattering data ($\lambda = 632.8\,\mathrm{nm}$, $n = 1.62 + i0.001$, $\delta = 0.223\,\mu\mathrm{m}$, $\ell = 1.42\,\mu\mathrm{m}$).

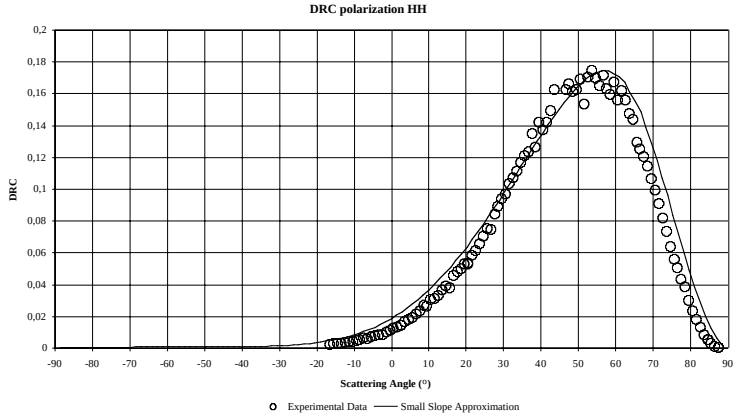

Figure 7a. Comparison of experimental data with the second-order small-slope approximation. 45° incident angle. Polarization HH, plane-of-incidence, bistatic, laser scattering data ($\lambda = 632.8\,\text{nm}$, $n = 1.62 + i0.001$, $\delta = 0.223\,\mu\text{m}$, $\ell = 1.42\,\mu\text{m}$).

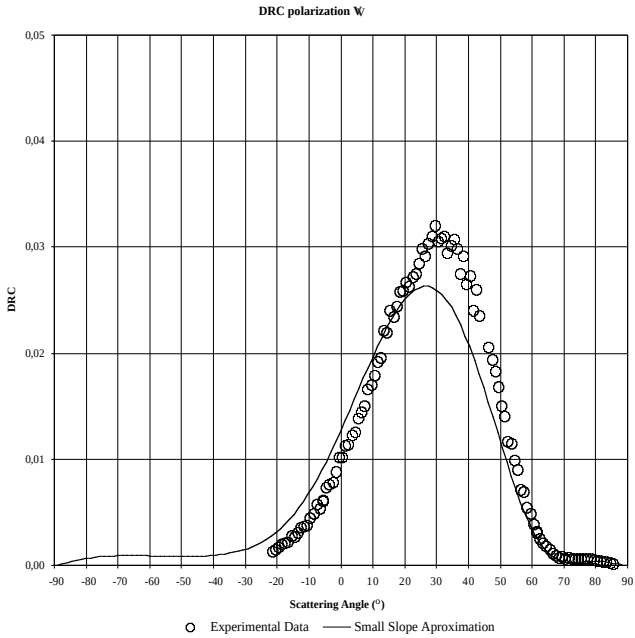

Figure 7b. Comparison of experimental data with the second-order small-slope approximation. 45° incident angle. Polarization VV, plane-of-incidence, bistatic, laser scattering data ($\lambda = 632.8\,\text{nm}$, $n = 1.62 + i0.001$, $\delta = 0.223\,\mu\text{m}$, $\ell = 1.42\,\mu\text{m}$).

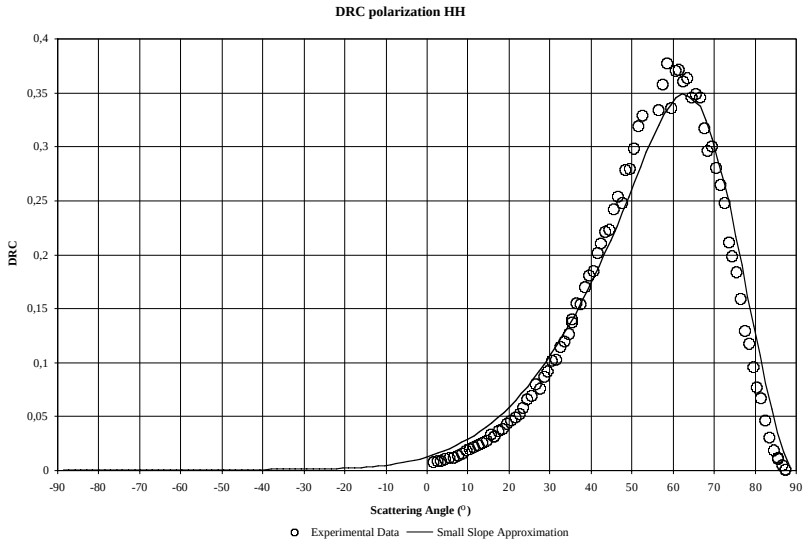

Figure 8a. Comparison of experimental data with the second-order small-slope approximation. 55° incident angle. Polarization HH, plane-of-incidence, bistatic, laser scattering data ($\lambda = 632.8\,\text{nm}$, $n = 1.62 + i0.001$, $\delta = 0.223\,\mu\text{m}$, $\ell = 1.42\,\mu\text{m}$).

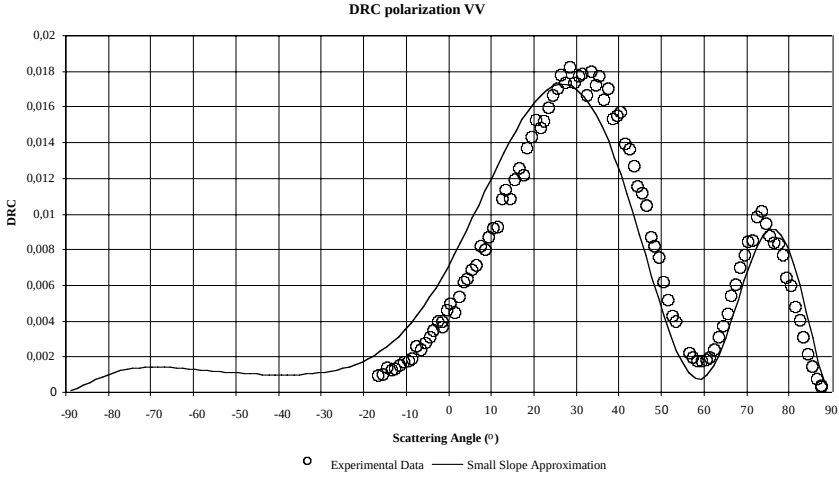

Figure 8b. Comparison of experimental data with the second-order small-slope approximation. 55° incident angle. Polarization VV, plane-of-incidence, bistatic, laser scattering data ($\lambda = 632.8\,\text{nm}$, $n = 1.62 + i0.001$, $\delta = 0.223\,\mu\text{m}$, $\ell = 1.42\,\mu\text{m}$).

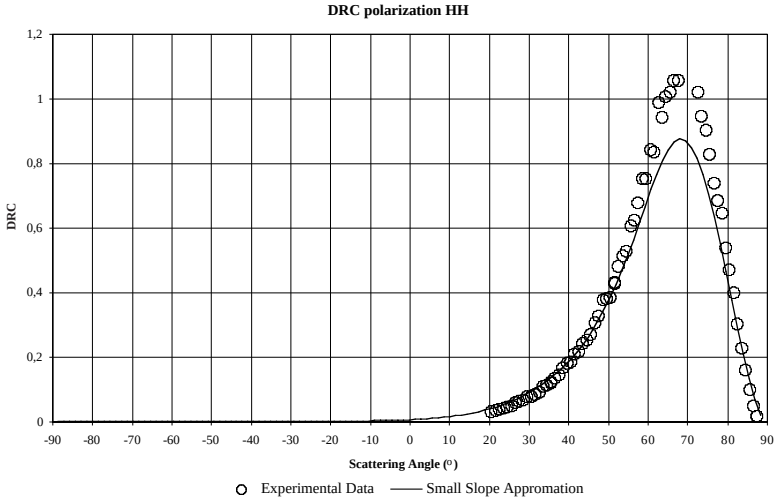

Figure 9a. Comparison of experimental data with the second-order small-slope approximation. 70° incident angle. Polarization HH, plane-of-incidence, bistatic, laser scattering data ($\lambda = 632.8\,\text{nm}$, $n = 1.62 + i0.001$, $\delta = 0.223\,\mu\text{m}$, $\ell = 1.42\,\mu\text{m}$).

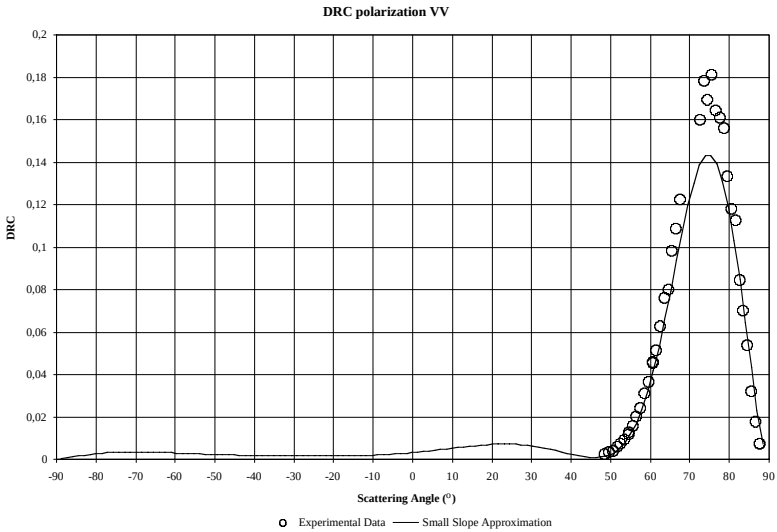

Figure 9b. Comparison of experimental data with the second-order small-slope approximation. 70° incident angle. Polarization VV, plane-of-incidence, bistatic, laser scattering data ($\lambda = 632.8\,\text{nm}$, $n = 1.62 + i0.001$, $\delta = 0.223\,\mu\text{m}$, $\ell = 1.42\,\mu\text{m}$).

of 70°, the predicted HH- and VV-polarized levels in the specular direction are slightly lower than the measurements. Although an excellent agreement between experimental data and model predictions is shown in previous figures, the sensitivity of the scattered levels to the definition of the correlation function is very important in the specular directions as we can see in Figures 10 and 11. In these figures, we compare Gaussian process with Gaussian and Lorentzian correlation functions for two incident angles 20° and 55°, in the plane-of-incidence and for the directions of polarization HH and VV. For the Gaussian and Lorentzian correlation functions, we take the following parameters: $\lambda = 632.8\,\text{nm}$, $n = 1.62 + i0.001$, $\delta = 0.223\,\mu\text{m}$ $\ell = 1.42\,\mu\text{m}$. For the Gaussian correlation function, we examine another case for the correlation length, which is given by $\ell = 1.562\,\mu\text{m}$. This value can represent a measure of accuracy with which the correlation length is estimated from the experimental data. We can note that the level and the lobe of the scattering cross-section depend on the accuracy of the correlation function estimation and the predictions of the SSA model depend on this estimation. In Figure 12, we give the polar diagrams of the incoherent scattering cross-section (DRC) calculated by the second-order small-slope approximation for the four polarization components and for a 55° incident angle. The Gaussian random rough surface is defined by the previous parameters. This representation gives the distribution of the scattered intensity in the azimuthal planes out of the plane-of-incidence for co- and cross-polarized components. The evolution of the cross-section at the "Brewster angle" in azimuthal planes is predicted by the Small-Slope Approximation method. In Figure 12, we can see that a phenomenon of "Brewster angle" occurs out of the plane of incidence for the vertical polarization of the laser wave.

3.3. Conducting Non Isotropic Surfaces with Non-Gaussian Correlation Function: Numerical Calculations

In this part, we consider an example of a randomly rough surface with a Gaussian height probability distribution and a non-Gaussian correlation function or a non-Gaussian power spectral density function (PSD). With this case, we demonstrate the capability of the second-order Small-Slope Approximation to calculate the scattered electromagnetic intensity by this non-Gaussian surface. The height probability distribution is chosen as a Gaussian function defined by its root mean square height δ given by $\mathbf{K}\delta = 0.1$, $\mathbf{K}$ is the incident wave number. The dielectric constant of the randomly rough surface $\varepsilon_r = -10.3 + i1.1$ is chosen to represent a constant with negative real part as in the case of metal at infrared wavelength. The incident wavelength

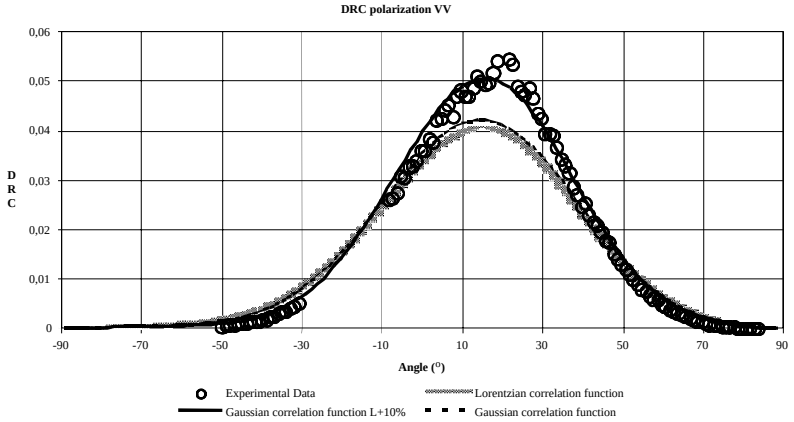

Figure 10a. Comparison of experimental data with the second-order small-slope approximation. 20° incident angle. Polarization HH, plane-of-incidence, bistatic, laser scattering data ($\lambda = 632.8\,\text{nm}$, $n = 1.62 + i0.001$, $\delta = 0.223\,\mu\text{m}$, $\ell = 1.42\,\mu\text{m}$).

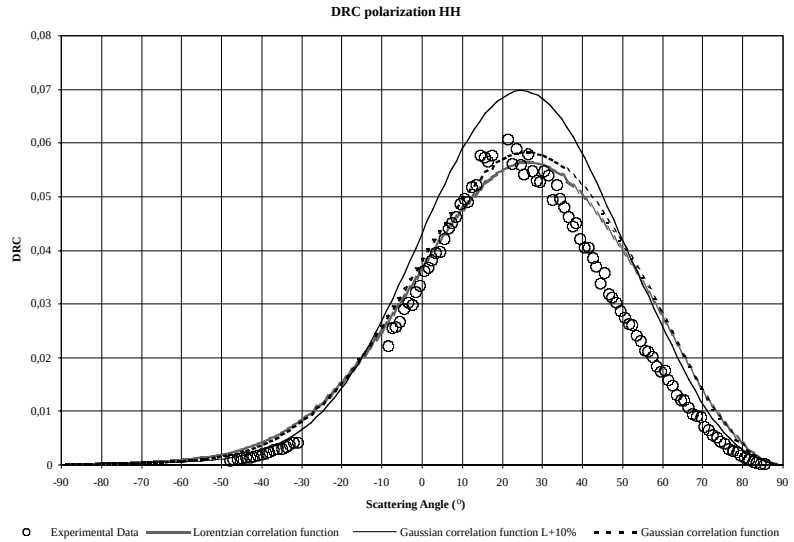

Figure 10b. Comparison of experimental data with the second-order small-slope approximation. 20° incident angle. Polarization VV, plane-of-incidence, bistatic, laser scattering data ($\lambda = 632.8\,\text{nm}$, $n = 1.62 + i0.001$, $\delta = 0.223\,\mu\text{m}$, $\ell = 1.42\,\mu\text{m}$).

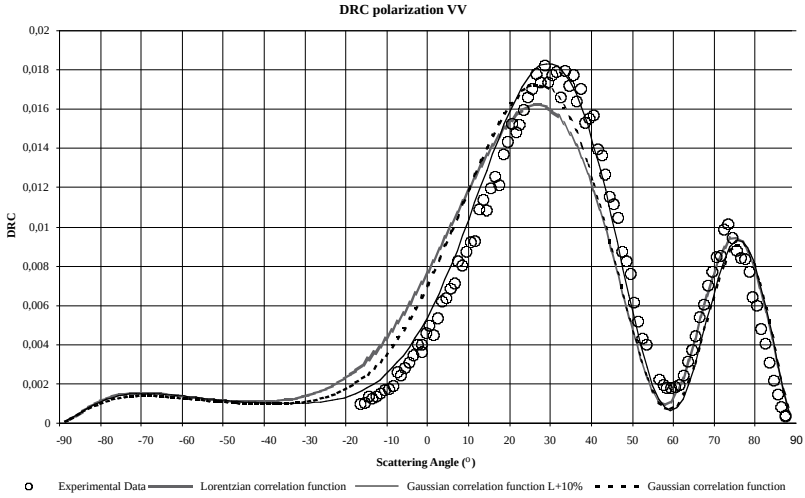

Figure 11a. DRC with different correlation functions. 55° incident angle. Polarization VV, plane-of-incidence, bistatic, laser scattering data ($\lambda = 632.8\,\text{nm}$, $n = 1.62 + i0.001$, $\delta = 0.223\,\mu\text{m}$, $\ell = 1.42\,\mu\text{m}$).

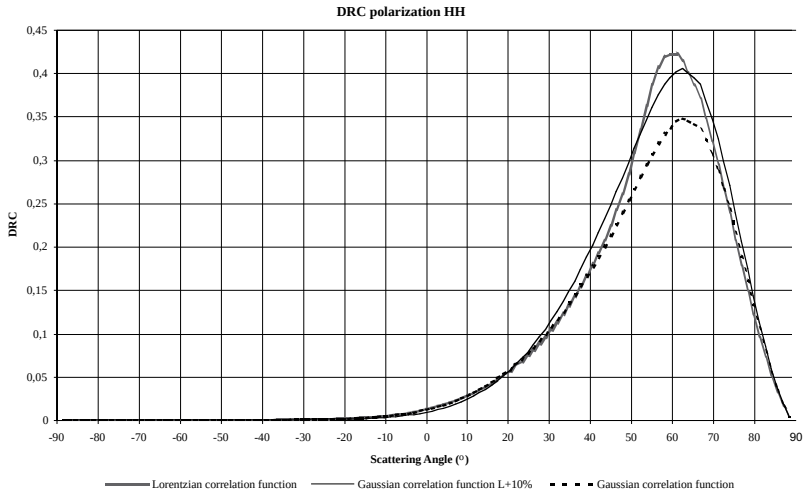

Figure 11b. DRC with different correlation functions. 55° incident angle. Polarization HH, plane-of-incidence, bistatic, laser scattering data ($\lambda = 632.8\,\text{nm}$, $n = 1.62 + i0.001$, $\delta = 0.223\,\mu\text{m}$, $\ell = 1.42\,\mu\text{m}$ or $\ell = 1.562\,\mu\text{m}$).

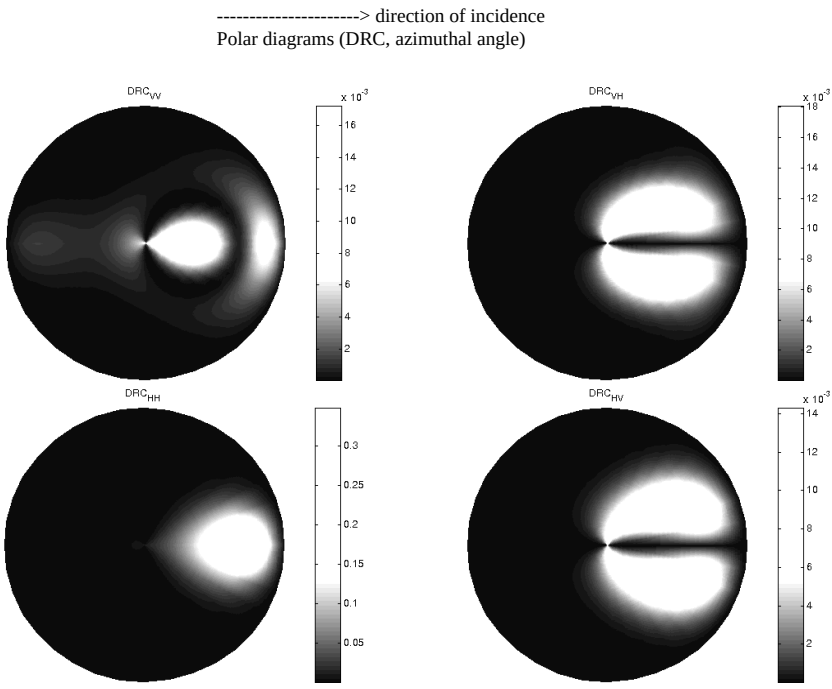

Figure 12. Polar diagrams of the DRC matrix (1/rad) calculated with second-order SSA for the polarization components HH,VH, HV, VV and for scattered angles in azimuthal planes. The angle of incidence is 55°. The plane-of-incidence is determined by the horizontal direction in the figures. The height probability distribution and the correlation function are Gaussian. The different parameters of the calculation are the following ones: ($\lambda = 632.8\,\mathrm{nm}$, $n = 1.62 + i0.001$, $\delta = 0.223\,\mu\mathrm{m}$, $\ell = 1.42\,\mu\mathrm{m}$).

is $\lambda = 10.6\,\mu\mathrm{m}$. We consider a power spectral density function defined by the superposition of a Gaussian isotropic component ($\mathbf{K}\ell = 6$ with $\mathbf{K}$ the incident wave number and ℓ the correlation length) with a directional angular component (in the direction of 45° in the spatial frequency domain with a spectrum width of 45°). The Figure 13 illustrates the non-isotropic PSD (power spectral density function) and the Figure 14 the normalized correlation function. The correlation function is characterized in the principal planes and in the plane at 135° by lobes, which give the non-isotropic nature to the surface. To illustrate the effects of the directional components of the correlation

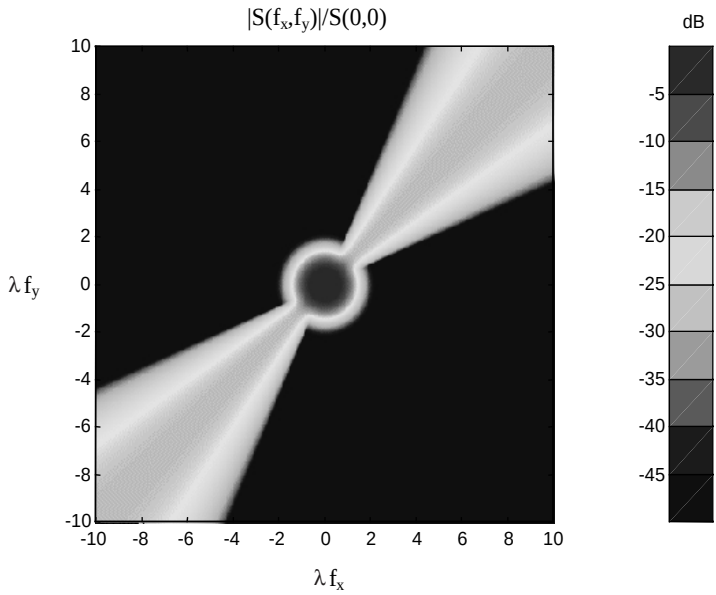

Figure 13. Normalized power spectral density function.

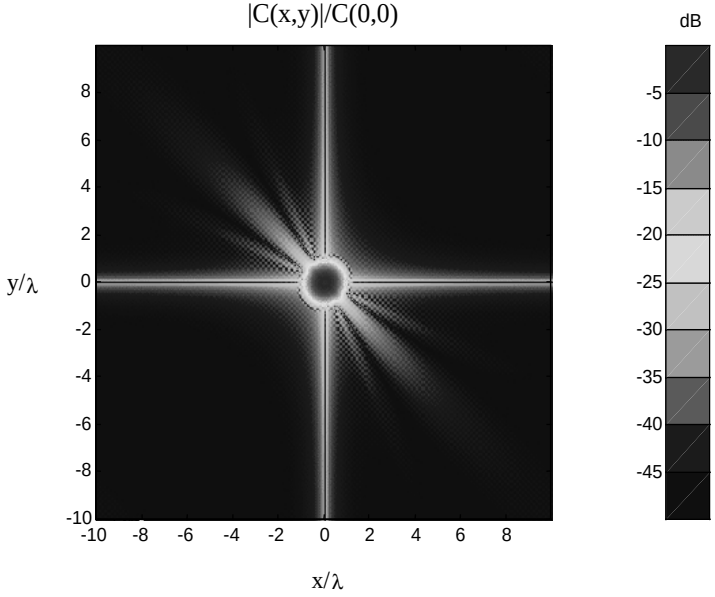

Figure 14. Normalized correlation function.

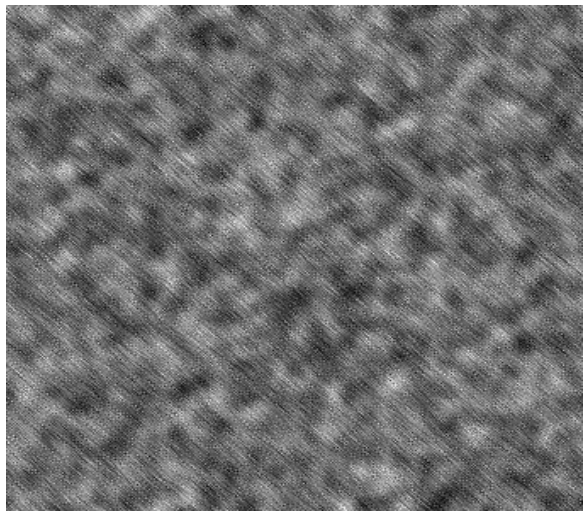

Figure 15. Realization of a randomly rough surface with the specified correlation function.

function and the power spectral density function, we have simulated in Figure 15 one realization of a random rough surface with the specified correlation function, using a white noise filtering technique. It must be noticed that the direction component of the correlation function introduces directional scratches on the random rough surface. The non-Gaussian roughness spectrum contains more high-frequency components than that of the Gaussian roughness surface defined by the Gaussian component of our non-Gaussian correlation function (Figures 13 and 14). The high frequency components in the non-Gaussian rough surface produce more small-scale roughness in the surface profile than a Gaussian rough surface. To verify this conclusion, we simulated one realization of a random rough surface (Figure 16) defined by the Gaussian component of the non-Gaussian spectrum (Figures 13 and 14). In Figure 17, we give the histogram of height distribution of the surface of the realized surface of Figure 15 and we compare it with the Gaussian distribution of the surface height with which we have defined the random rough surface, we can verify the excellent correlation between the Gaussian distribution and the histogram of the realization. We consider a bistatic configuration with an incident elevation angle of 45°. The plane (Ox, Oz) determines the plane-of-incidence. We calculate the incoherent scattering cross-section. To normalize the scattering cross-section, we divide it by the

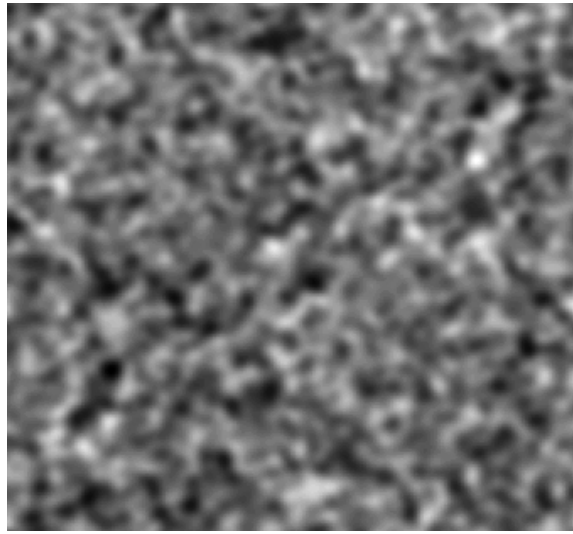

Figure 16. Realization of a randomly rough surface with the Gaussian correlation function.

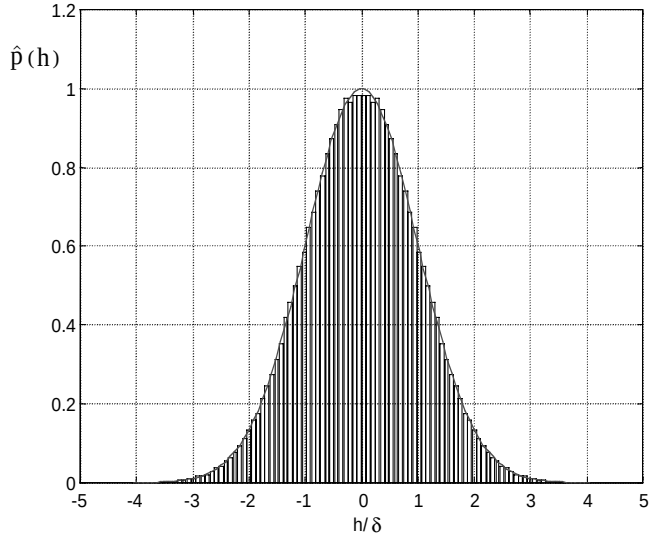

Figure 17. Normalized histogram of surface data given by the surface described in Figure 15 in comparison with the theoretical Gaussian distribution $\hat{p}(h) = p(h)\delta\sqrt{2\pi})$.

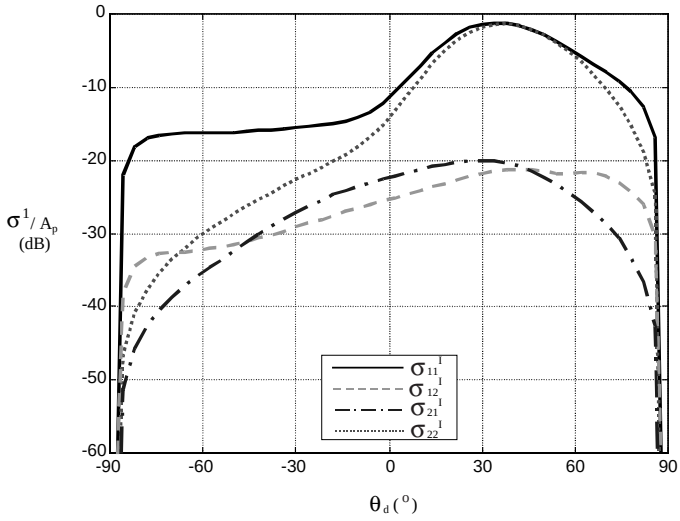

Figure 18. Scattered incoherent components in the plane-of-incidence (Ox, Oz) for the non-Gaussian correlation function. A bistatic configuration is considered, the incident elevation angle is 45°. The scattered incoherent components are calculated as a function of the scattered elevation angle.

projection (A_p) of the illuminated surface area (radar footprint) onto the reference plane. In Figures 18 and 19, the vertical polarization is defined by 1 and the horizontal polarization is defined by 2. The co-polarized components VV and HH of the incoherent scattering cross-section matrix are represented by 11 and 22, the cross-polarized components VH and HV respectively by 12 and 21. In Figure 18, the scattered incoherent components are calculated in the plane-of-incidence as a function of the scattered elevation angle. In Figure 19, the scattered components are calculated in the 45°-azimuthal plane. In the plane-of-incidence, we observe the depolarization of the diffuse field given by the cross-polarized components of the scattering cross-section matrix, which are not negligible compared to the co-polarized terms. The second-order SSA method predicts depolarization in the plane-of-incidence in this complex case. In the 45°-azimuthal plane, we observe similar patterns for the co- and cross-polarized components in the case of the non-Gaussian power spectral density function. These results confirm that the second-order SSA method is able to treat the problem of scattering by two-dimensional random rough surfaces with non-Gaussian correlation function and to give valuable information on the scattering phenomena obtained with this kind of surface.

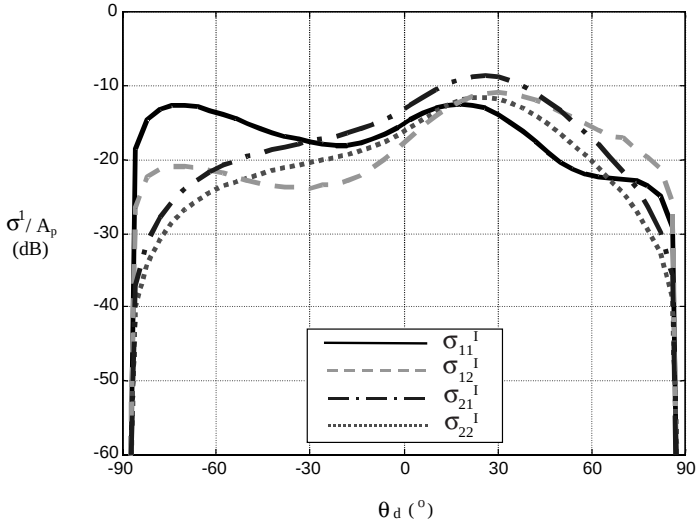

Figure 19. Scattered incoherent components in the 45°-azimuthal plane for the non-Gaussian correlation function. A bistatic configuration is considered, the incident elevation angle in the plane-of-incidence (Ox, Oz) is 45°. The scattered incoherent components are calculated as a function of the scattered elevation angle.

4. CONCLUSION

This paper has addressed the problem of scattering of a vector wave from a dielectric or metallic rough surface with small slopes. The method of second-order small-slope expansion was applied to the vector case for two homogeneous media described by their permeability and permittivity. The rough boundary separating these two volumes can be described by non-Gaussian correlation functions. The SSA formulation of the vector case for two-dimensional surfaces leads to expressions, which are numerically tractable for this three-dimensional scattering problem. This SSA formulation provides accurate numerical results, which were compared successfully in this paper with experimental data from metallic and dielectric two-dimensional randomly rough surfaces. The SSA formulation gives remarkably accurate results and describes all the polarized states of the scattered intensity. A numerical example with non-Gaussian correlation function is presented in this paper. It can be alleged that many scattering problems by metallic or dielectric two-dimensional randomly rough surfaces with small slopes can solved with the SSA formulations and the associated

numerical code. Thus, the SSA appears to be one of the best-adapted methods for a large scope of three-dimensional scattering problems. With the small-slope approximation, we can investigate phenomena like absorption by metallic surface, scattering by surfaces with non-Gaussian correlation function, Brewster effect, etc. The non-local small-slope approximation gives the back-scattering enhancement. The small-slope approximation is a self-consistent theory, which can be used for computing the coherent and incoherent back-scattering cross-sections of more complex objects with metallic or dielectric randomly rough surfaces.

REFERENCES

1. Tsang, L., J. A. Kong, K. H. Ding, and C. A. Ao, *Scattering of Electromagnetic Waves, Numerical Simulations,* Wiley Series in Remote Sensing, Wiley Interscience, New York, 2001.
2. Bourlier, C., G. Berginc, and J. Saillard, "Theoretical study of the Kirchhoff integral from a two-dimensional randomly rough surface with shadowing effect: application to the backscattering coefficient for a perfectly-conducting surface," *Waves in Random Media*, Vol. 11, 91–118, 2001.
3. Bourlier, C., G. Berginc, and J. Saillard, "Bistatic scattering coefficient from one- and two-dimensional random surfaces using the stationary phase and scalar approximation with shadowing effect: comparisons with experiments and application to the sea surface," *Waves in Random Media,* Vol. 11, 119–147, 2001.
4. Fitzgerald, R. M. and A. A. Maradudin, "A reciprocal phase-perturbation theory for rough surface scattering," *Waves Random Media*, Vol. 4, 275–296, 1994.
5. Bahar, E., "Full wave solutions for the depolarization of the scattered radiation fields by rough surfaces of arbitrary slope," *IEEE Trans. Antennas Propag.,* Vol. 29, 443–454, 1981.
6. Fung, A. K., *Microwave Scattering and Emission Models and Their Applications,* Artech House, Boston, MA, 1994.
7. Hsieh, G. Y., A. K. Fung, G. Nesti, A. J. Sieber, and P. Coppo, "A further study of the IEM surface scattering model," *IEEE Geos. Rem. Sens.,* Vol. 35, No. 4, 901–909, 1997.
8. Hsieh, G. Y., "Effects of bistatic multiple surface scattering from perfectly conducting surface," *Electromagnetics,* Vol. 20, No. 2, 99–124, 2000.
9. Hsieh, G. Y., "Prediction of IEM model for backscattering enhancement," *Electromagnetics,* Vol. 20, No. 3, 205–231, 2000.

10. Jin, Y.-Q., "Multiple scattering from a randomly rough surface," *J. Appl. Phys.,* Vol. 63, No. 5, 1286–1292, 1988.
11. Jin, Y.-Q., "Backscattering enhancement from a randomly rough surface," *Physical Review,* Vol. B42, No. 16, 9819–9829, 1990.
12. Ishimaru, A. and S. Chen, "Scattering from very rough metallic and dielectric surfaces: a theory based on a modified Kirchhoff approximation," *Waves Random Media*, Vol. 1, S91–S107, 1991.
13. Ishimaru, A., C. Le, Y. Kuga, L. A. Sengers, and T. K. Chan, "Polarimetric scattering theory for high slope rough surfaces," *PIER, Progress In Electromagnetic Research,* J. A. Kong (ed.), Vol. 14, 1–36, EMW, 1996.
14. Alvarez-Perez, J. L., "An extension of the IEM/IEMM surface scattering model," *Waves Random Media,* Vol. 11, 307–330, 2001.
15. Milder, D. M., "An improved formalism for wave from rough surfaces," *J. Acoust. Soc. Am.,* Vol. 89, 529–541, 1991.
16. Voronovich, A. G., "Small slope approximation in wave scattering by rough surfaces," *Sov. Phys.-JETP,* Vol. 62, 65–70, 1985.
17. Voronovich, A. G., *Wave Scattering from Rough Surfaces,* Springer Series on Wave Phenomena, 2nd edition, Springer, Berlin, 1998.
18. Voronovich, A. G., "Small-slope approximation for electromagnetic wave scattering at a rough interface of two dielectric half-space," *Wave in Random Media,* Vol. 4, 337–367, 1994.
19. Voronovich, A. G., "Non local small-slope for wave scattering from rough surfaces," *Wave in Random Media,* Vol. 6, 151–167.
20. Broschat, S. L. and E. I. Thorsos, "An investigation of the small slope approximation for scattering from rough surfaces, Part I," Theory J. Acoust. Soc. Am., Vol. 89, 2082–2093, 1995.
21. Berginc, G, Y. Béniguel, and B. Chevalier, "Small-slope approximation method: higher order contributions for scattering from conducting 3D surfaces," *Proceedings of SPIE,* P.T. C. Chen, Z.-H. Gu, and A. A. Maradudin (eds.), Rough Surface Scattering and Contamination, Vol. 3784, 207–217, 1999.
22. Chevalier, B. and G. Berginc, "Small-slope approximation method: scattering of a vector wave from 2D dielectric and metallic surfaces with Gaussian and non-Gaussian statistics," *Proceedings of SPIE,* Z.-H. Gu and A. A. Maradudin (eds.), Scattering and Surface Roughness III, Vol. 4100, 22–32, 2000.
23. Berginc, G. and Y. Béniguel, "Extension of the small-slope approximation method for 3D scattering cross-section calculation of a rough convex object," *PIERS Proceedings, Nantes,* 582, 1998.

24. Tsang, L. and J. A. Kong, *Scattering of Electromagnetic Waves, Advanced Topics,* Wiley Series in Remote Sensing, Wiley Interscience, New York, 2001.
25. O'Donnel, K. A. and E. R. Mendez, "Experimental study of scattering characterized random surfaces," *J. Opt. Soc. Am.,* Vol. 4, No. 7, 1194–1205, 1987.
26. Bahar, E. and B. S. Lee, "Radar scatter cross section for two-dimensional random rough surfaces — full wave solutions and comparisons with experiments," *Wave in Random Media,* Vol. 6, 1–23, 1996.
27. Hernandez-Walls, C. E. I. and E. R. Mendez, "Scattering by randomly two-dimensional dielectric surfaces," *Proceedings of SPIE,* Vol. 3426, 164–170, 1998.
28. Calvo-Perez, O., "Diffusion des ondes électromagnétiques par un film diélectrique rugueux hétérogène. Etude expérimentale et modélisation," Ph.D. Thesis, Ecole Centrale de Paris, French, 1999.